Available online at www.sciencedirect.com
ScienceDirect
Trans. Nonferrous Met. Soc. China 25(2015) 2817−2826
Transactions of Nonferrous Metals Society of China
www.tnmsc.cn

Effect of Zr additions and annealing temperature on electrical conductivity and hardness of hot rolled Al sheets

N. A. BELOV[1], A. N. ALABIN[1], I. A. MATVEEVA[2], D. G. ESKIN[3,4]

1. Department of Casting Technologies, National Research and Technological University "MISIS", Leninsky Prospect 4, Moscow 119049, Russia;
2. UC RUSAL, 13/1, Nikoloyamskaya streat, Moscow 109240, Russia;
3. Brunel University London, BCAST, Kingston Lane, Uxbridge UB8 3PH, UK;
4. Tomsk State University, Tomsk, Prospect Lenina 36, 634050, Russia

Received 9 November 2014; accepted 20 January 2015

Abstract: The influence of annealing cycles up to 650 °C on the specific conductivity and hardness (HV) of hot-rolled sheets of Al alloys containing up to 0.5% Zr (mass fraction) was studied. Using analytical calculations of phase composition and experimental methods (scanning electron microscopy, transmission electron microscopy, electron microprobe analysis, etc), it is demonstrated that the conductivity depends on the content of Zr in the Al solid solution which is the minimum after holding at 450 °C for 3 h. On the other hand, the hardness of the alloy is mainly caused by the amount of nanoparticles of the $L1_2$ (Al_3Zr) phase that defines the retention of strain hardening. It is shown that the best combination of electrical conductivity and hardness values can be reached within an acceptable holding time at the temperature about 450 °C.

Key words: Al−Zr alloys; Al_3Zr nano-particles; phase composition; electrical conductivity; annealing temperature

1 Introduction

Al alloys are widely used for the production of wires for overhead power transmission lines where the light weight in combination with reasonable electrical conductivity makes Al preferable over heavy Cu [1]. In recent years, the power industry has increased the requirements for thermally stable Al alloys that should combine high electrical conductivity and sufficient strength preserved after heating up to 300 °C. The latter requirement rules out the use of unalloyed Al (AA1350) as its recrystallization-onset temperature is low (less than 250 °C) [2]. One of the solutions of this problem is to develop low-alloyed Al alloys with Zr additions [3−7], e.g., 0.5%–2% Zr [5], 0.23%−0.35% Zr [6] and about 0.3% Zr [7] (mass fraction). A number of widely known companies, such as Lamifil (Belgium), 3M (USA), J-Power Systems (Japan) and others, conduct research and development in the field of heat-resistant wires, where Al−Zr alloys are used with international standard IEC 62004 [8] and ASTM B941-10 [9].

Wire rods for manufacturing of electrical cables are typically manufactured by continuous casting and rolling (CCR), in particular on rolling mills Properzi [10] and Southwire [11]. The desired characteristics of Al−Zr wire (specific conductivity, strength and thermal stability) depend considerably on the processing schedule of a wire rod, which includes the Zr content, casting conditions, rolling regime and, especially, the heat treatment cycle. According to the experimental results of TACER et al [12], the conductivity of an Al–0.25%Zr (mass fraction) alloy reaches the peak values after annealing at 450–450 °C for 60–80 h. BELOV et al [13] found out that the resistivity of cold-rolled sheets containing 0.3%–0.6% Zr (mass fraction) is primarily determined by the Zr content in the Al solid solution.

The optimization of the process parameters is a difficult task that is caused by the complexity of CCR process (Fig. 1) which significantly differs from the conventional processing routes when the casting of billets and the subsequent deformation are separated in time and space. The positive influence of Zr on the hardness (as a measure of thermal stability) is caused by

Foundation item: Project (RMEF157814X0004) supported by the Ministry of Education and Science of the Russian Federation
Corresponding author: N. A. BELOV; Tel: +7-495-9511928; E-mail: nikolay-belov@yandex.ru
DOI: 10.1016/S1003-6326(15)63907-3

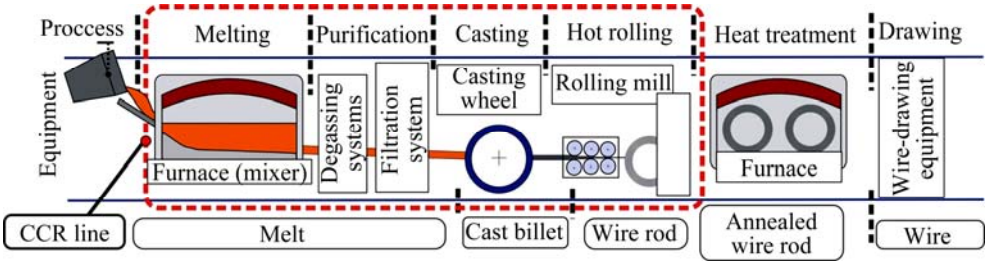

Fig. 1 Main technological stages of wire rod and wire production

the nanoparticles of $L1_2$ (Al_3Zr) phase formed in a wire rod upon the decomposition of a supersaturated Al solid solution (α(Al)) during the annealing process [14−29]. KNIPLING et al [14] found out that these nanoparticles start to precipitate between 350 and 375 °C, achieving a peak microhardness of 420 MPa at 425–450 °C. Small additions of other elements, particularly rare earth, such as Er [21,23,28,29] and Yb [22,24,27], do not significantly affect the strengthening.

The annealing process is a key factor which determines the objectives to produce hot-rolled sheets of Al alloys containing up to 0.5% Zr (mass fraction) under conditions approaching typical commercial CCR machines, and to study the influence of annealing temperature (up to 650 °C), the content of Zr in α(Al) and the quantity of $L1_2$ (Al_3Zr) nanoparticles on the electrical conductivity, hardness and phase composition of these alloys.

2 Experimental

The sheets of experimental Al alloys containing 0.1%−0.5% Zr (mass fraction), and the wire rods of an Al−Zr alloy (0.24% Zr, 0.22% Fe, 0.07% Si, mass fraction) were the main objects of this research. The wire rods were produced by the CCR technology at the IrkAZ (RUSAL) Smelter (Irkutsk, Russia) [30]. The experimental alloys were prepared in an electric resistance furnace in a graphite-clay crucible with an primary Al (99.7% purity) as the base material. Zr (up to 0.5%) was introduced into the melt in the form of an Al–15%Zr (mass fraction) master alloy produced by Intermix Met. The additions were made at 850–900 °C, i.e., above the liquidus of the alloy containing 0.5% Zr which is about 810 °C [13, 25]. The flat ingots with sizes of 40 mm×120 mm×180 mm (Fig. 2) were cast in a steel mold at the cooling rate of about 10 °C/s. The sheets with 5 mm in thickness were produced from these flat ingots according to the technological scheme shown in Fig. 3. The chemical compositions of the alloys, particularly the content of Zr in the alloy, were determined with an emission spectrometer ARL 4460 and are given in Table 1. The

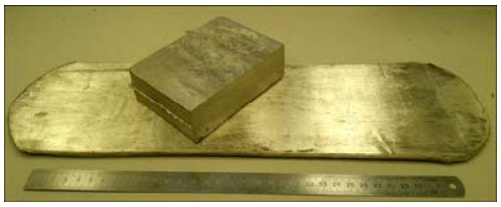

Fig. 2 Experimental ingot and Al–Zr alloy sheet

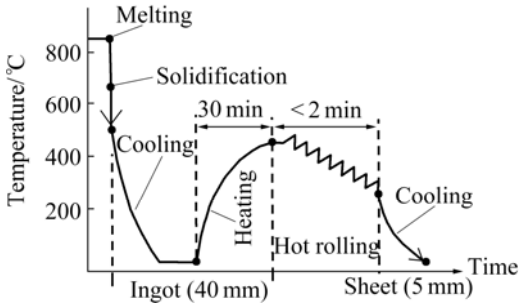

Fig. 3 Temperature−technological scheme of experimental sheets production

Table 1 Chemical compositions of experimental alloys (mass fraction, %)

Alloy	Si	Fe	Zr	Al
00Zr	0.073	0.140	−	Bal.
02Zr	0.072	0.139	0.180	Bal.
03Zr	0.074	0.131	0.283	Bal.
04Zr	0.080	0.140	0.380	Bal.
05Zr	0.075	0.133	0.476	Bal.

sheets were annealed in a muffle electric furnace Nabetherm using step cycles in the range of 250−650 °C (Table 2) with an accuracy of temperature maintenance ±2 °C.

The specific electrical conductivity (EC) was measured by eddy-current testing using a VE-26NP device with high purity Al (99.99%) as an additional standard. The Vickers hardness (HV) was determined in a Wilson Wolpert 930 N hardness machine with a load of 50 N. The measurements of electrical conductivity and hardness were carried out for each heat treatment cycle,

Table 2 Annealing regimes of Al–Zr sheets

Designation	Annealing regime
T300	300 °C, 3 h
T350	T300+(350 °C, 3 h)
T400	T350+(400 °C, 3 h)
T450	T400+(450 °C, 3 h)
T500	T450+(500 °C, 3 h)
T550	T500+(550 °C, 3 h)
T600	T550+(600 °C, 3 h)
T650	T600+(650 °C, 3 h)

making at least 5 measurements for each value. The statistical analysis of the results was performed and the average data are reported.

The structure was examined by optical microscopy (OM, Axiovert 200 MMAT), transmission electron microscopy (TEM, JEM−2100), scanning electron microscopy (SEM, TESCAN VEGA 3) and electron microprobe analysis (EMPA, OXFORD AZtec). The polished samples cut from the ingots and sheets (Fig. 2) were studied. Mechanical polishing (Struers Labopol-5) was used as well as electrolytic polishing, as these methods complement one another and enable the complete observation of the microstructure. The electrolytic polishing was performed using 12 V in an electrolyte containing 6 parts of ethanol, 1 part of $HClO_4$ and 1 part of glycerin. The thin foils for transmission electron microscopy (TEM) were prepared by electrolitic thinning in a perchloric acid–alcohol solution and studied at 160 kV.

The calculations of phase composition, particularly, the mass fraction of Al_3Zr phase and the content of Zr in the Al solid solution at different temperatures $w(Zr)_{\alpha(Al)}$ were made using Thermo-Calc software (version TCW-5, database TTAL5) [31].

3 Results

The metallographic analysis of ingots (Fig. 4) shows that the microstructures are quite similar irrespective of the Zr content in the experimental alloys. The reason is the complete dissolution of Zr in the Al solid solution during solidification at a sufficiently high cooling rate, while the contents of Fe and Si do not vary much between the alloys (Table 1). The observed microstructures are typical of commercial Al: inclusions of Al_8Fe_2Si phase in a shape of skeletal fragments or streaks [31] at the α(Al) dendritic cells boundaries (Fig. 4(c)). However, a noticeable grain refinement is observed with increasing the Zr content. Particularly, the average linear grain size in alloy 02Zr is ~300 m (Fig. 4(a)), while in alloy 05Zr, it is below 100 m (Fig. 4(b)). As it is well known, Zr that dissolved in α(Al) strongly reduces electrical conductivity [2]. Assuming that the major factor determining the electrical conductivity (EC) of alloys is the content of Zr in the Al solid solution, the dependence of EC on the Zr content in α(Al) is derived. Figure 5 shows this dependence in the

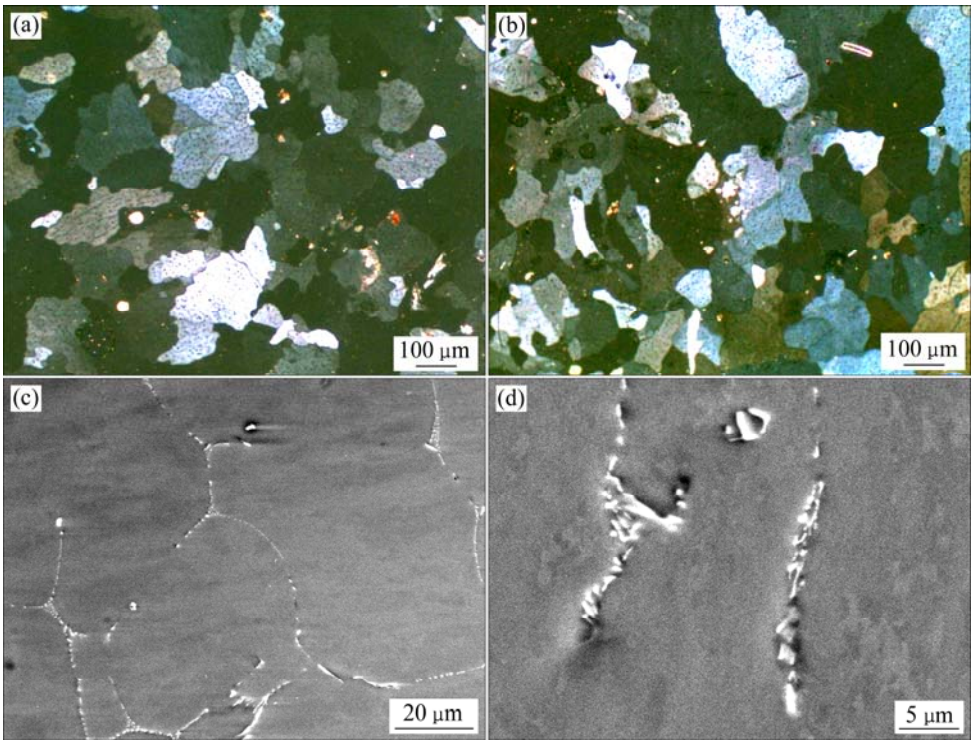

Fig. 4 OM images of as-cast Al−0.48%Zr (a) and Al−0.18%Zr (b) ingots and SEM images of as-cast Al−0.48%Zr ingot (c) and hot rolled Al−0.48%Zr sheet (d)

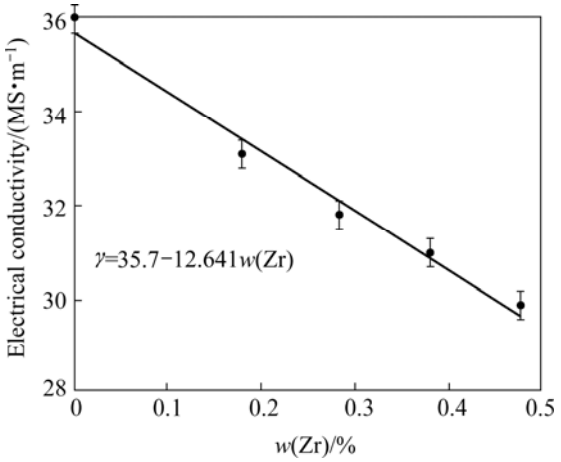

Fig. 5 Electrical conductivity versus Zr content in as-cast ingot

as-cast state as a linear function with the coefficient of ~12.6 that characterizes the decrease of EC with the addition of 1% Zr:

$$\gamma = 35.7 - 12.641\ w(\mathrm{Zr})_{\alpha(\mathrm{Al})} \quad (1)$$

where γ is the value of EC and $w(\mathrm{Zr})_{\alpha(\mathrm{Al})}$ is the content of Zr in α(Al).

The value of $w(\mathrm{Zr})_{\alpha(\mathrm{Al})}$ was determined from the experimental results. In this case, all Zr in the alloy is assumed to dissolve into the solid solution during solidification, hence in the as-cast state, the value of $w(\mathrm{Zr})_{\alpha(\mathrm{Al})}$ should coincide with the content of Zr in the alloy (w(Zr)), as no primary intermetallics are observed in the structure. The linear dependence shown in Fig. 5 means that the effect of grain size (Figs. 4(a) and (b)) is much smaller than that of Zr content in the Al solid solution on the electrical conductivity.

During rolling, a fibrous structure with elongated inclusions of the Fe-containing phase are formed (Fig. 4(d)). The mass ratio of Fe to Si in these particles according to EMPA is 4–5 (like in the Al_8Fe_2Si phase). Zr does not influence the structure of alloys after hot rolling, as can be revealed in a light microscope.

According to the Al−Zr phase diagram, almost all experimental alloys (disregarding Fe and Si impurities) fall in the solid state into the two-phase region α(Al)+Al_3Zr (Fig. 6). Alloys 02Zr and 03Zr that single-phased at 650 °C make an exception. The alloy 02Zr falls into the single-phase area also at 600 °C. From Fig. 6, it follows that the annealing of all the alloys should result in the decomposition of the supersaturated α(Al) and the formation of Al_3Zr phase precipitates.

The dependence of EC of the alloys on the temperature at the last step of annealing has complex character (Fig. 7(a)). Unlike the unalloyed Al where the value of EC changes only slightly (the scatter of data is comparable with the experimental accuracy), the alloys with Zr demonstrate significant changes. The changes are especially great at the maximum content of Zr in the

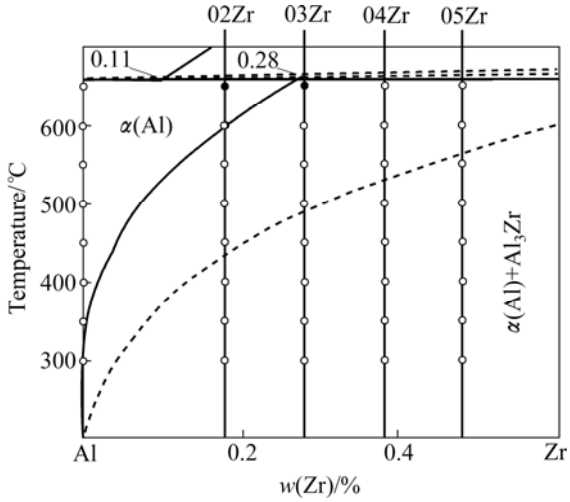

Fig. 6 Phase diagram of Al−Zr alloy

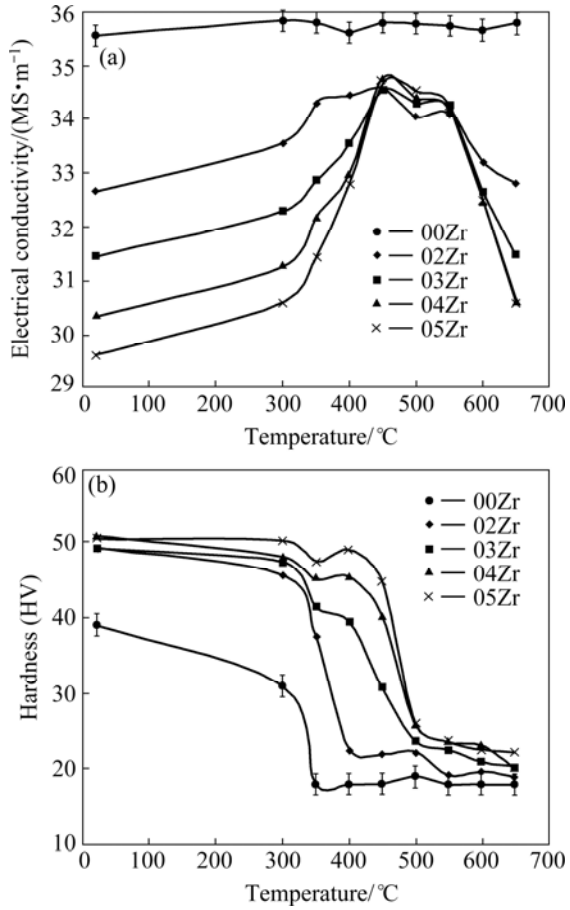

Fig. 7 Electrical conductivity (a) and hardness (b) of Al–Zr alloys versus temperature at last step of annealing

alloy, i.e., the difference in EC values in alloy 05Zr across the whole range of annealing temperatures is 5.4 MS/m (or ~15%). The annealing up to 350 °C leads to slight increase of EC, with the differences between alloys remaining. The value of EC reaches the maximum after annealing at the T450 cycle. It should be noted that in this state, the difference in EC between Zr-containing alloys is minimal. Further increasing the temperature

leads to the decrease of EC, the difference between alloys becomes greater again but to a lesser extent as compared with the as-cast state.

The dependence of hardness on the temperature at the last step of annealing (Fig. 7(b)) shows that the work hardening of all Zr-containing alloys remains up to 300 °C. It should be noted that unalloyed Al at this temperature completely softens and its hardness does not exceed HV 20. As the temperature increases, the influence of the content of Zr in the alloy on the hardness becomes essential. In the alloys 02Zr and 03Zr, the noticeable softening is observed at 350 °C and 400 °C, respectively. In more concentrated alloys 04Zr and 05Zr, the hardness remains at a rather high level up to 450 °C. At 500 °C and higher, all alloys strongly soften and the difference between them is leveled.

The metallographic analysis of the annealed sheets shows that the formation of recrystallized grains coincides with the softening, while higher values of hardness, with the fibrous (close to initial) structure (Fig. 8). The resistance to recrystallization is caused by the formation of the nanoparticles of Al_3Zr phase, as revealed in the TEM images (Fig. 9). As Fig. 9(c) shows, the average size of these particles does not exceed 10 nm at the T450 cycle. Upon heating over 450 °C, the particles coarsen and then transform to the stable $D0_{23}$ (Al_3Zr) phase which can be seen in an SEM image. For example, the precipitates of the stable phase in alloy 05Zr reach 1 μm in size after annealing at the T650 cycle (Fig. 10(a)). In alloys 02Zr and 03Zr annealed at the T650 cycle, these particles are absent due to the complete dissolution of Zr in α(Al) in full compliance with the Al−Zr phase diagram (Fig. 6). The needle-shaped particles (Fig. 10(b)) contain Fe but no Si, as revealed by the SEM−EPMA. It may be explained by the phase transformation during annealing at 650 °C according to the equilibrium Al–Fe–Si phase diagram [32,33].

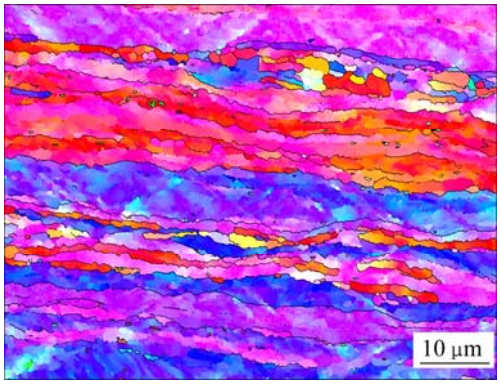

Fig. 8 Grain structure of alloy sheet 05Zr after annealing at T450 cycle

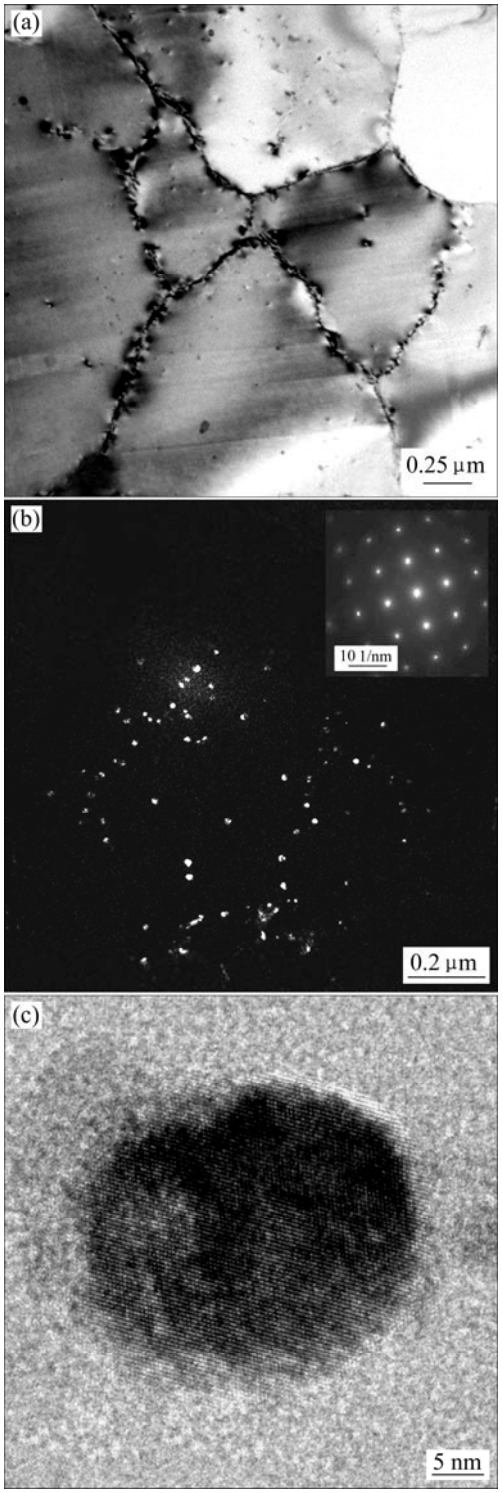

Fig. 9 TEM images of alloy sheet 05Zr after annealing at T450 cycle: (a) Bright image; (b) Dark image; (c) HRTEM image

The industrial relevance of the obtained results is verified using an industrially produced wire rod containing 0.24% Zr. The CCR equipment of IrkAZ does not allow the melt temperature near the casting wheel (Fig. 1) to be above ~750 °C, so it prevents the use of Al–Zr alloys with a higher Zr content. Multi-stage (T1) and one-stage (T2) cycles are considered. The multi-

stage was conducted similarly to the experiment, i.e., with holding for 3 h at each step (Table 2), one-stage annealing was carried out at 300, 350, 400, 450 and 500 °C with holding for 10 h, respectively. as shown in Fig. 11, in both cases, the maximum value of conductivity is observed at 450 °C. At the same time, the multi-step annealing slightly increases the EC in comparison with the one-step heating with the EC values of 35.4 and 35.1 MS/m, respectively. In the case of lower temperatures, the required holding time significantly increases, whereas at higher temperatures, the conductivity decreases due to the increased solubility of Zr in α(Al).

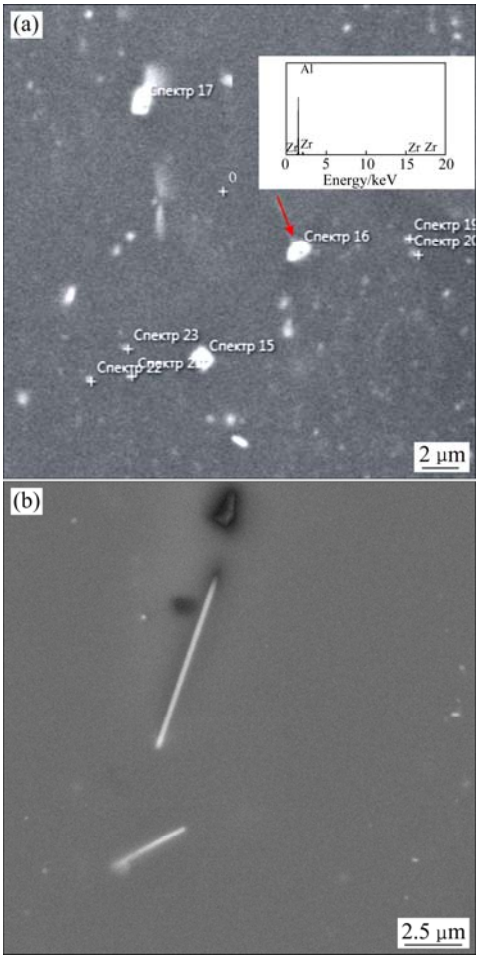

Fig. 10 SEM images of alloy sheet 05Zr after annealing at T650 cycle: (a) Coarsen Al_3Zr precipitates (Points 15, 16 and 17); (b) Al_3Fe needle-like particles

4 Discussion

The structural and phase transformations during the annealing process were estimated through conductivity and hardness measurement (Fig. 7) and also by calculation. The quantitative values characterizing the phase composition at specific temperature are given in Table 3. The calculations were carried out for both stable

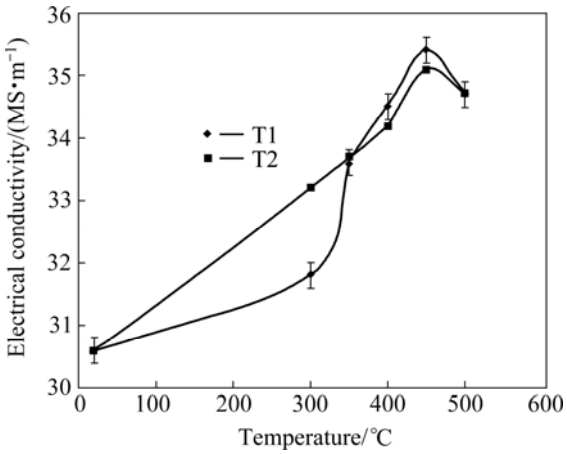

Fig. 11 Effect of annealing temperature on electrical conductivity of wire rod (0.24% Zr) (T1: multi-stage annealing; T2: one-stage annealing)

and metastable equilibrium. From Table 3, it is evident that the solubility of Zr in α(Al) considerably increases at temperatures over 400 °C. Moreover, in the case of metastable equilibrium, the solubility is significantly higher.

As it follows from the dependences shown in Fig. 7(a), when using multi-stage annealing, the electrical conductivity reaches the maximum value at 450 °C which possibly correlates with the maximum depletion of Zr in the Al solid solution. However, it does not correlate with the calculated data for the metastable equilibrium showing that the content of Zr in α(Al) at the given temperature is considerable (Table 3).

As an explanation of the dependences shown in Fig. 7, the content of Zr in α(Al) was inverse-calculated using the coefficient of linear correlation between $w(Zr)_{\alpha(Al)}$ and γ (Fig. 5) or experimentally determined values of γ (in sheets). Thus other factors, in particular, the number of Al_3Zr precipitates and their size, were neglected. The results of the calculation given in Table 4 show that in the T350 state, the calculated values of $w(Zr)_{\alpha(Al)}$ are significantly higher than those shown in Table 3. Hence, it follows that annealing at 350 °C for 3 h is obviously insufficient for achieving the equilibrium (in this case it is metastable). On the other hand, in the T450 state, the calculated values of $w(Zr)_{\alpha(Al)}$ are higher than those obtained according to the stable Al−Zr phase diagram, but are much lower than those for the metastable equilibrium. As the precipitates of the $L1_2$ phase are experimentally revealed under this condition (Fig. 9), it may be assumed that the calculations according to database TTAL5 base give higher values of $w(Zr)_{\alpha(Al)}$ for the metastable option ("overestimate"). According to the study of SIGLI [34], the metastable solubility of Zr inα(Al) at 450 °C is about0.1% (mass fraction) (twice as less as that shown in Table 3). In the

Table 3 Calculated values of Zr solubility in Al solid solution ($w(Zr)_{\alpha(Al)}$) and mass fraction of Al_3Zr phase ($w(Al_3Zr)$) for alloys at various temperatures

Alloy	Temperature/°C	Stable phase equilibria ($D0_{23}$)		Metastable phase equilibria ($L1_2$)	
		$w(Zr)_{\alpha(Al)}$/%	$w(Al_3Zr)$/%	$w(Zr)_{\alpha(Al)}$/%	$w(Al_3Zr)$/%
02Zr	300	0.003	0.33	0.037	0.27
	350	0.009	0.32	0.072	0.20
	400	0.019	0.30	0.125	0.10
	450	0.038	0.27	0.180	0
	500	0.068	0.21	0.180	0
	550	0.113	0.13	0.180	0
	600	0.178	<0.01	0.180	0
	650	0.180	0	0.180	0
03Zr	300	0.003	0.52	0.037	0.46
	350	0.009	0.51	0.072	0.39
	400	0.019	0.49	0.125	0.29
	450	0.038	0.46	0.203	0.14
	500	0.068	0.40	0.283	0
	550	0.113	0.32	0.283	0
	600	0.178	0.19	0.283	0
	650	0.267	0.02	0.283	0
04Zr	300	0.003	0.71	0.037	0.65
	350	0.009	0.70	0.072	0.58
	400	0.019	0.68	0.125	0.48
	450	0.038	0.65	0.203	0.33
	500	0.068	0.59	0.309	0.14
	550	0.113	0.51	0.380	0
	600	0.178	0.38	0.380	0
	650	0.267	0.21	0.380	0
05Zr	300	0.003	0.90	0.037	0.83
	350	0.009	0.89	0.072	0.76
	400	0.019	0.87	0.125	0.66
	450	0.038	0.84	0.203	0.51
	500	0.068	0.78	0.309	0.31
	550	0.113	0.69	0.449	0.05
	600	0.178	0.57	0.476	0
	650	0.267	0.40	0.476	0

Table 4 Calculated values of Zr solubility in Al solid solution ($w(Zr)_{\alpha(Al)}$) and mass fraction of Al_3Zr phase ($w(Al_3Zr)$) in alloys after annealing

Alloy	$w(Zr)_{\alpha(Al)}$/%			$w(Al_3Zr)$/%		
	T350	T450	T550	T350	T450	T550
02Zr	0.060	0.079	0.106	0.226	0.191	0.140
03Zr	0.185	0.085	0.099	0.185	0.374	0.347
04Zr	0.232	0.066	0.099	0.279	0.592	0.530
05Zr	0.285	0.073	0.099	0.360	0.760	0.711

T550 state, the calculated values of $w(Zr)_{\alpha(Al)}$ correspond well to the stable phase diagram of Al−Zr that allows us to assume the formation of $D0_{23}$ phase instead of $L1_2$. The mass fraction of secondary precipitates of the Al_3Zr phase ($w(Al_3Zr)$) was calculated using the difference between $w(Zr)$ and $w(Zr)_{\alpha(Al)}$, as well as the content of Zr in the Al_3Zr phase (53%, mass fraction). As Table 4 shows, the quantity of $L1_2$ precipitates is the maximum in the alloy 05Zr in the T450 state, when the best combination between hardness and electrical

conductivity is reached. On the other hand, in alloy 02Zr, the T350 state is most optimal when the $w(Zr)_{\alpha(Al)}$ value is the minimum and $w(Al_3Zr)$, on the contrary, is the maximum. After annealing at the T550 cycle, all alloys possess low hardness. It can be considered that the number of $D0_{23}$ precipitates does not significantly affect the hardness at 550 °C and higher temperatures.

The results of calculations given above allow us to explain the influence of the Zr content in the alloy on the conductivity and hardness at the specific cycle of annealing (Fig. 12). In the initial state, the dependence between γ and w(Zr) is close to be linear with a small deviation towards decrease at the increased w(Zr) values (Fig. 12(a)). It can be explained that during hot rolling, Zr generally remains in α(Al) and only in alloys 04Zr and 05Zr, there is a chance of some decomposition (Table 4). The dependence of γ−w(Zr) for T350 state is similar to that for the initial state, but the values of γ are higher by approximately 1.5–2 MS/m, that indicates the partial precipitation of Zr from α(Al). The most interesting pattern is observed in the T450 state where the value of γ does not significantly depend on w(Zr). This suggests that the influence of the secondary precipitates of $Al_3Zr(L1_2)$ on the EC is insignificant as

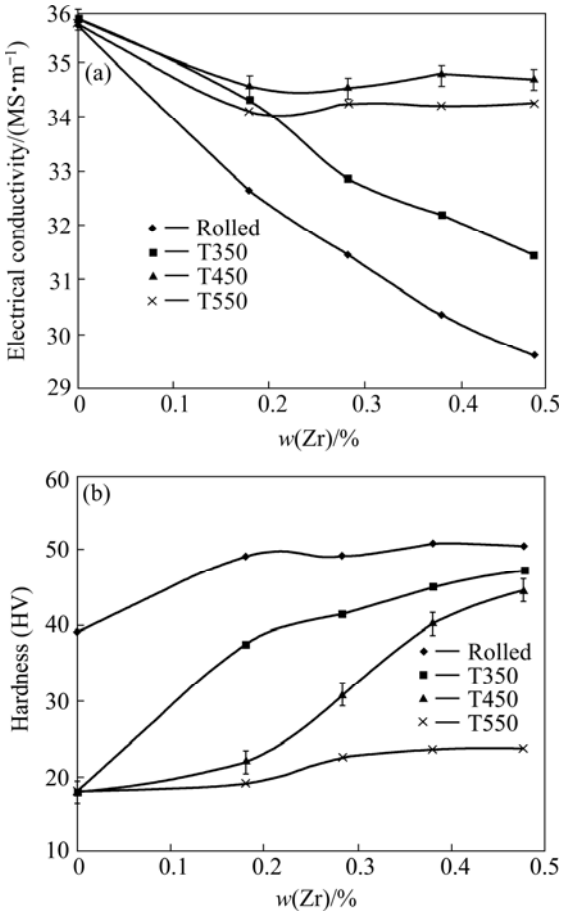

Fig. 12 Electrical conductivity (a) and hardness (b) of Al–Zr alloys sheet versus Zr content in alloy

compared with that of the Zr content in α(Al) (Fig. 5). As a result, the alloys in the T450 state differ only by a number of Al_3Zr precipitates (Table 4). After annealing on the T550 cycle, the difference between the alloys is also insignificant that can be explained by the close values of EC. The dependences of hardness on the content of Zr in the alloy (Fig. 12(b)) can be explained by the quantity of $L1_2$ (Al_3Zr) nanoparticles (Fig. 9) that define the strain hardness retention. The influence of Zr content in the alloy is most considerably pronounced after annealing at the T450 cycle when the amount of the $L1_2$ phase in all alloys (except 02Zr) is the maximum.

To obtain the highest conductivity, the entire Zr has to be bound into the Al_3Zr phase, and for this purpose, the annealing temperature has to be the lowest as this corresponds to the minimum equilibrium values of $w(Zr)_{\alpha(Al)}$ (Table 3). However, because of the slow diffusion of Zr in α(Al) at the temperatures of 300−350 °C, the required time for dissolution is too long [14]. It is obvious that this way is unacceptable for practical applications. Besides, it is necessary to take into account that the heat-resistant alloys should be subjected to stabilizing heat treatment at a temperature exceeding the maximum working temperature. From the obtained experimental data and results of calculation, it can be concluded that the combination of conductivity and hardness, which has close correlation with the strength properties, can be achieved if the temperature of heat treatment is in the range of 400−450 °C, and the content of Zr is 0.3% and higher (shown in Fig. 7, alloys 03Zr, 04Zr, and 05Zr).

5 Conclusions

1) The influence of annealing cycles up to 650 °C on the specific conductivity and hardness of hot-rolled sheets of Al alloys containing up to 0.5% Zr was studied under the conditions approaching those realized at industrial continuous casting and rolling units.

2) By using analytical calculations and experimental methods, it is demonstrated that the conductivity depends on the content of Zr in the Al solid solution, which is the maximum after holding at 450 °C for 3 h. On the other hand, the hardness of the alloy is mainly caused by the amount of nanoparticles of the $L1_2$ (Al_3Zr) phase that defines the retention of strain hardening.

3) It is shown that the best combination of conductivity, strength and hardness values can be reached within an acceptable holding time at the temperature about 450 °C. At lower temperatures, the necessary holding time significantly increases, whereas at higher temperatures, there is a decrease of

conductivity that is related to a greater solubility of Zr in α(Al).

References

[1] POLMEAR I J. Light metals: From traditional alloys to nanocrystals [M]. 4th ed. Burlington: Elsevier, 2006.

[2] HATCH J E. Aluminum: Properties and physical metallurgy [M]. Ohio: ASM, 1984.

[3] KNYCH T, JABŁONSKI M, SMYRAK B. New aluminium alloys for electrical wires of fine diameter for automotive industry [J]. Archives of Metallurgy and Materials, 2009, 54: 671−676.

[4] ZHOU W W, CAI B, LI W J, LIU Z X, YANG S. Heat-resistant Al−0.2Sc−0.04Zr electrical conductor [J]. Materials Science and Engineering A, 2012, 552: 353−358.

[5] BRUBAK J P, EFTESTOL B, LADISZLAIDESZ F. Aluminium alloy, a method of making it and an application of the alloy: US, 5067994 [P]. 1991−11−26.

[6] KENICHI S, KAZUHISA Y, YASUMASA H,TAKASI K, MINORU Y. High conductive heat-resistant aluminum alloy: US, 4402763 [P]. 1983−09−06.

[7] BELOV N A, ALABIN A N, TOLEUOVA A. Comparative analysis of alloying additives as applied to the production of heat-resistant wires [J]. Metal Science and Heat Treatment, 2011, 53: 455−459.

[8] IEC 62004 Edition 1.0. Thermal-resistant aluminium alloy wire for overhead line conductor [S].

[9] ASTM B941−10. Standard specification for heat resistant aluminum-zirconium alloy wire for electrical purposes [S].

[10] PROPERZI I. Machine for the continuous casting of metal rods: US, 2659949 [P]. 1953−11−24.

[11] SCHOERNER R J. Method of fabricating aluminum alloy rod: US, 3670401 [P]. 1972−06−20.

[12] TECER H, ACER E, EROL H, GÜNDÜZ M. Effect of aging on conductivity of heat resistant overhead line conductors [J]. Materials Science Forum, 2013, 765: 783−787.

[13] BELOV N A, ALABIN A N, PROKHOROV A Y. The influence that a zirconium additive has on the strength and electrical resistance of cold-rolled aluminum sheets [J]. Russian Journal of Non-Ferrous Metals, 2009, 50: 357−362.

[14] KNIPLING K E, KARNESKY R A, LEE C P, DUNAND D C, SEIDMAN D N. Precipitation evolution in Al−0.1Sc, Al−0.1Zr and Al−0.1Sc−0.1Zr (at.%) alloys during isochronal ageing [J]. Acta Materialia, 2010, 58: 5184−5195.

[15] CLOUET E, BARBU A, LAE L, MARTIN G. Precipitation kinetics of Al_3Zr and Al_3Sc in aluminum alloys modeled with cluster dynamics [J]. Acta Materialia, 2005, 53: 2313−2325.

[16] DESCHAMP A, GUYO P. In situ small-angle scattering study of the precipitation kinetics in an Al−Zr−Sc alloy [J]. Acta Materialia, 2007, 55: 2775−2783.

[17] LEFEBVRE W, DANOIX F, HALLEM H, FORBORD B, BOSTEL A, MARTHINSEN K. Precipitation kinetic of Al_3(Sc,Zr) dispersoids in aluminium [J]. Journal of Alloys and Compounds, 2009, 470: 107−110.

[18] FORBORD B, LEFEBVRE W, DANOIX F, HALLEM H, MARTHINSEN K. Three dimensional atom probe investigation on the formation of Al_3(Sc,Zr)-dispersoids in aluminium alloys [J]. Scripta Materialia, 2004, 51: 333−337.

[19] KNIPLING K E, DUNAND D C, SEIDMAN D N. Precipitation evolution in Al−Zr and Al−Zr−Ti alloys during aging at 450–600 °C [J]. Acta Materialia, 2008, 56: 1182−1195.

[20] BOOTH-MORRISON C, MAO Z, DIAZ M, DUNAND D C, WOLVERTON C, SEIDMAN D N. Role of silicon in accelerating the nucleation of Al_3(Sc,Zr) precipitates in dilute Al−Sc−Zr alloys [J]. Acta Materialia, 2012, 60: 4740−4752.

[21] BOOTH-MORRISON C, SEIDMAN D N, DUNAND D C. Effect of Er additions on ambient and high-temperature strength of precipitation-strengthened Al−Zr−Sc−Si alloys [J]. Acta Materialia, 2012, 60: 3643−3654.

[22] VAN DALEN M E, GYGER T, DUNAND D C, SEIDMAN D N. Effects of Yb and Zr microalloying additions on the microstructure and mechanical properties of dilute Al−Sc alloys [J]. Acta Materialia, 2011, 59: 7615−7626.

[23] BOOTH-MORRISON C, DUNAND D C, SEIDMAN D N. Coarsening resistance at 400 °C of precipitation-strengthened Al−Zr−Sc−Er alloys [J]. Acta Materialia, 2011, 59: 7029−7042.

[24] PENG G, CHEN K, FANG H, CHEN S. A study of nanoscale Al_3(Zr,Yb) dispersoids structure and thermal stability in Al−Zr−Yb alloy [J]. Materials Science and Engineering A, 2012, 535: 311−315.

[25] BELOV N A, ALABIN A N, ESKIN D G, ISTOMIN-KASTROVSKIY V V. Optimization of hardening of Al−Zr−Sc casting alloys [J]. Journal of Materials Science, 2006, 41: 5890−5899.

[26] FORBORD B, LEFEBRE W, DANOIX F, HALLEM H, MARTHINSEN K. Three dimensional atom probe investigation on the formation of Al_3(Sc,Zr)-dispersoids in aluminium alloys [J]. Scripta Materialia, 2004, 51: 333−337.

[27] PENG G, CHEN K, FANG H, CHEN S. A study of nanoscale Al_3(Zr,Yb) dispersoids structure and thermal stability in Al−Zr−Yb alloy [J]. Materials Science and Engineering A, 2012, 535: 311−315.

[28] WEN S P, GAO K Y, HUANG H, WANG W, NIE Z R. Precipitation evolution in Al−Er−Zr alloys during aging at elevated temperature [J]. Journal of Alloys and Compounds, 2013, 574: 92−97.

[29] LI H Y, GAO Z H, YIN H, JIANG H F, SU X J, BIN J. Effects of Er and Zr additions on precipitation and recrystallization of pure aluminum [J]. Scripta Materialia, 2013, 68: 59−62.

[30] IrkAZ (RUSAL) [EB/OL]. http://www.rusal.ru.

[31] Databases released by Thermo-Calc Software Company [EB/OL]. http://www.thermocalc.com.

[32] BELOV N A, AKSENOV A A, ESKIN D G. Multicomponent phase diagrams: Applications for commercial aluminum alloys [M]. Kidlington: Elsevier, 2005.

[33] CHEN H, CHEN Q, DU Y, BRATBERG J, ENGSTRÖM A. Update of Al−Fe−Si, Al−Mn−Si and Al−Fe−Mn−Si thermodynamic descriptions [J]. Transactions of Nonferrous Metals Society of China, 2014, 24(7): 2041−2053.

[34] SIGLI C. Zirconium solubility in aluminum alloys [C]// Proc International Conference on Aluminium Alloys 2004. Brisbane, Australia: ICAA9, 2004: 1353−1358.

Zr 添加量和退火温度对热轧 Al 板电导率和硬度的影响

N. A. BELOV[1], A. N. ALABIN[1], I. A. MATVEEVA[2], D. G. ESKIN[3,4]

1. Department of Casting Technologies, National Research and Technological University “MISIS”, Leninsky Prospect 4, Moscow 119049, Russia;
2. UC RUSAL, 13/1, Nikoloyamskaya streat, Moscow 109240, Russia;
3. Brunel University London, BCAST, Kingston Lane, Uxbridge UB8 3PH, UK;
4. Tomsk State University, Tomsk, Prospect Lenina 36, 634050, Russia

摘　要：研究退火温度高达 650 °C 的循环退火对 Zr 含量高达 0.5%(质量分数)的热轧 Al 合金板的比电导率和硬度的影响。相图成分计算和扫描电镜、透射电镜、电子显微探针分析结果表明，Al 板的电导率取决于 Al 固溶体中的 Zr 含量，在 450 °C 退火 3 h 时，Al 固溶体中的 Zr 含量最低。另一方面，合金板的硬度主要取决于 $L1_2(Al_3Zr)$ 相纳米颗粒的数量。在 450 °C 退火一定的时间可得到最好的电导率和硬度值。

关键词：Al−Zr 合金；Al_3Zr 纳米颗粒；相成分；电导率；退火温度

(Edited by Mu-lan QIN)